# Mechanistic insights into a hydrate contribution to the Paleocene-Eocene carbon cycle perturbation from coupled thermohydraulic simulations

**T. A. Minshull[1*], H. Marín-Moreno[2,3], D. I. Armstrong M[c]Kay[1,4] and P. A. Wilson[1]**

[1]National Oceanography Centre Southampton, University of Southampton, Southampton, UK

[2]Istituto Nazionale di Oceanografia e di Geofisica Sperimentale, Trieste, Italy

[3]National Oceanography Centre, Southampton, UK.

[4]Geography and Environment, University of Southampton, Southampton, SO17 1BJ, UK

[*]Corresponding author email: tmin@noc.soton.ac.uk

**Key Points**

1. Rapid ocean warming, as during the PETM, can lead to rapid hydrate dissociation, but methane release to the ocean is delayed and gradual.

2. In our models, most of the methane released from hydrate remains in the sediment pores, with only a small fraction reaching the ocean.

3. A late Paleocene hydrate inventory of at least 4000 Pg is needed to explain the PETM carbon isotope excursion.

**Abstract**

During the Paleocene-Eocene Thermal Maximum (PETM), the carbon isotopic signature ($\delta^{13}C$) of surface carbon-bearing phases decreased abruptly by at least 2.5 to 3.0 ‰. This

carbon isotope excursion (CIE) has been attributed to widespread methane hydrate dissociation in response to rapid ocean warming. We ran a thermohydraulic modeling code to simulate hydrate dissociation due to ocean warming for various PETM scenarios. Our results show that hydrate dissociation in response to such warming can be rapid but suggest that methane release to the ocean is modest and delayed by hundreds to thousands of years after the onset of dissociation, limiting the potential for positive feedback from emissions-induced warming. In all of our simulations at least half of the dissociated hydrate methane remains beneath the seabed, suggesting that the pre-PETM hydrate inventory needed to account for all of the CIE is at least double that required for isotopic mass balance.

## 1. Introduction

Methane is a strong greenhouse gas that oxidizes in about a decade to carbon dioxide and can thereby continue to impact climate for many millennia [*Archer and Brovkin*, 2008]. Methane hydrates are stable at high pressures and low temperatures and can accumulate beneath the deep ocean over millions of years. If the overlying ocean warms, hydrate that has accumulated beneath the seabed over a long period can dissociate and methane may be released into the ocean. Present-day venting into the oceans at several locations may be attributed to such a mechanism [*Darnell and Flemings*, 2015; *Phrampus and Hornbach*, 2012; *Phrampus et al.*, 2014; *Westbrook et al.*, 2009], though the origin of the methane involved remains controversial [*Berndt et al.*, 2014]. Widespread hydrate dissociation has the potential to lead to a positive feedback in which the released methane and its oxidation product, carbon dioxide, enhance warming [*Archer and Buffett*, 2005]. On the centennial to millennial timescales over which this feedback is hypothesized to operate, however, several processes below the seafloor have the potential to slow, shut down or even reverse methane release in response to thermal dissociation of gas hydrate. In addition to the long-recognized

effects on heat propagation of thermal diffusion [e.g., *Dickens et al.*, 1995], it is important to consider the role of latent heat in hydrate dissociation [e.g., *Thatcher et al.*, 2013], and the effects of of bubble transport and biogeochemical consumption [e.g., *Boetius and Wenzhöfer*, 2013] on methane release from the seabed.

The early Paleogene was characterized by several "hyperthermals", which appear to represent geologically brief (< 200 kyr) episodes of globalwarming and massive carbon input associated with decreases in the stable oxygen and carbon isotope composition of biogenic carbonate [*Littler et al.*, 2014; *Sexton et al.*, 2011; *Zachos et al.*, 2008]. The most extreme and the best-studied of these events, the Paleocene-Eocene Thermal Maximum (PETM; Figure 1), is characterized by an increase in the global mean surface ocean temperature of ~5 °C, warming of the surface ocean locally by up to 9 °C, shoaling of the depth in the ocean of total carbonate dissolution in seafloor sediments by at least 2 km in the Atlantic, the extinction of many species of benthic foraminifera and a prominent carbon isotopic excursion (CIE) involving a decrease in $\delta^{13}C$ of carbon-bearing phases by at least 2.5-3.0 ‰ [*Dickens*, 2011; *Dunkley Jones et al.*, 2013; *Foster et al.*, 2013; *Zachos et al.*, 2005; *Zeebe et al.*, 2009]. These observations indicate rapid perturbation of the exogenic carbon cycle through the release of buried organic carbon.

Mass balance considerations suggest that between 2,000 and 13,000 Pg of carbon rich in the $^{12}C$ isotope must have been released in less than 10,000 years at the start of this event [*Cui et al.*, 2011; *Dickens*, 2011; *Dickens et al.*, 1995; *Panchuk et al.*, 2008; *Zeebe et al.*, 2009]. Most current estimates for the duration of the initial isotope excursion are in the range 1 to 10 kyr; the bimodal isotope distribution seen in records from individual shells in expanded sections point to the short end member of this range [*Zachos et al.*, 2007] but there is little support for

75 a much shorter (decadal) perturbation [*Wright and Schaller*, 2013]. As a result, the PETM has
76 been proposed as a partial analogue to current anthropogenic emissions and climate change,
77 where the total mass of carbon input is comparable but where anthropogenic rates of carbon
78 emission are an order of magnitude faster [*Zeebe et al.*, 2016]. Several sources of carbon have
79 been hypothesized to be involved including permafrost or kerogen and volcanism-induced
80 thermogenic methane during the emplacement of the North Atlantic Volcanic Province [*Cui*
81 *et al.*, 2011; *DeConto et al.*, 2012; *Svensen et al.*, 2004] but the longest standing hypothesized
82 mechanism involves widespread dissociation of methane hydrates [*Dickens*, 2011; *Dickens et*
83 *al.*, 1995; *Sluijs et al.*, 2007; *Thomas et al.*, 2002].
84
85 Because PETM modeling efforts to date have been motivated largely by a need to understand
86 the basic mass balance [*Dickens*, 2011] they have, understandably, employed relatively
87 simplistic numerical analysis. Commonly, for example, it is assumed that the timescale for
88 methane release is primarily controlled by the diffusion of heat into the subsurface [e.g., *Katz*
89 *et al.*, 2001], and that all the methane from hydrate dissociation rises rapidly to the seabed. *Xu*
90 *et al.* [2001] developed a model for the PETM that explicitly considers fluid flow and
91 methane transport. However, that model (i) does not account for the effects of latent heat,
92 which slows the downward propagation of heat [*Thatcher et al.*, 2013] or for salinity
93 variations that perturb the phase boundary, (ii) only considers methane transport in solution,
94 without bubbles, and (iii) assumes high fluid flow rates more representative of active than
95 passive margins. Thus, enhanced methane transport into the ocean results primarily from
96 increased methane solubility in warmer pore fluids. A more recent simulation of the PETM
97 incorporates the effects of latent heat, but not the effects of pressure and salinity variations
98 resulting from hydrate dissociation [*Zeebe*, 2013]. That simulation assumes that upon
99 dissociation, methane is rapidly released into the ocean, and therefore does not consider the

100 physical and biogeochemical processes that may slow its ascent and perhaps even prevent its
101 arrival at the seafloor. Here we employ a more sophisticated numerical model of sub-seabed
102 processes that was developed to understand present-day methane release and to predict future
103 release [*Marín-Moreno et al.*, 2013; *Reagan and Moridis*, 2007; *Stranne et al.*, 2016;
104 *Thatcher et al.*, 2013]. We simulate the response of hypothetical slope sediment sequences
105 representative of those likely to have contained methane hydrate during the Palaeocene to
106 some simple PETM warming scenarios to show how methane transport and dissolution
107 processes influence the timescale and magnitude of methane generation and release into the
108 ocean.
109
110 **2. Method and Results**
111 We ran one-dimensional simulations using the thermohydraulic fully coupled
112 TOUGH+Hydrate code [*Moridis et al.*, 2012]. This code numerically solves coupled
113 equations of heat and mass balance, and hence can model the non-isothermal gas release,
114 phase behavior and flow of fluids and heat in gas hydrate bearing geological systems. The
115 continuum balance equations of each of the mass components (water, methane and salt) and
116 heat are discretized in space by the integral finite difference method [e.g*., Narasimhan and*
117 *Witherspoon*, 1976] and in time by first order finite difference. The resultant set of coupled,
118 non-linear, algebraic equations are solved by Newton-Raphson iteration, approximating the
119 Jacobian matrix by numerical differentiation, and using sparse direct matrix methods or
120 iteratively with a preconditioned conjugate gradient method [*Moridis and Pruess*, 1995]. We
121 assumed equilibrium conditions for hydrate formation and dissociation and that the mass
122 components water, methane and salt were partitioned between four possible phases: hydrate
123 (water and methane), aqueous (water, methane, salt), gas (water and methane), and ice
124 (water). We modeled heat exchanges due to conduction, convection, hydrate formation and

dissociation, and methane and salt dissolution. We used Darcy's law for the flow of water and methane in the aqueous and gas phases, respectively, and for the advective transport of methane and salt in the aqueous phase. For the molecular diffusive transport of methane and salt within the aqueous phase we used a Fick's type law. Calculated seabed methane emissions include contributions from both methane bubble flow and dissolved methane. TOUGH+Hydrate is a well-documented code and has been employed in several works to model warming-induced hydrate dissociation [e.g., *Marín-Moreno et al.*, 2013; *Reagan and Moridis*, 2007; *Stranne et al.*, 2016; *Thatcher et al.*, 2013]. However, for completeness, further details of this code and our approach to its use are given in the supporting information.

Our models used parameters matching those of *Zeebe* [2013] and *Marín-Moreno et al.* [2013] (supporting information). Model sensitivity to a wide range of parameters has been explored previously [*Marín-Moreno et al.*, 2013; *Thatcher et al.*, 2013]. The permeability and the irreducible gas saturation (IGS), above which free gas can flow, are key parameters controlling the onset of methane emissions and amount emitted. If permeabilities appropriate to hemipelagic sediments are used, hydrate dissociation leads to a build-up of pore pressure that would be sufficient to fracture such sediments [*Stranne et al.*, 2016; *Thatcher et al.*, 2013]. The released version of TOUGH+Hydrate can neither simulate the formation of fractures nor, in a one-dimensional model, account for pre-existing fractures. The formation of fractures has been tackled recently by *Marín-Moreno et al.* [2015a] and *Stranne et al.* [2016] using an *a posteriori* offline approach following *Daigle and Dugan's* [2010] normalized overpressure ratio criterion. Here we model porous flow in pristine hemipelagic sediments using an intrinsic permeability of $10^{-16}$ $m^2$, and approximate fracture flow by modeling porous flow with an enhanced intrinsic permeability of $10^{-13}$ $m^2$ (supporting

information). Our simulations compute the evolution of intrinsic permeability with porosity according to *Xu*'s *et al*., [2004] relationship, the methane and water relative permeabilities according to a modified version of *Stone*'s [1970] first three-phase relative permeability method, the capillary pressure according to *van Genuchten*'s [1980] law, and the bulk thermal conductivity of the sediments according to *Moridis et al.* [2005] (supporting information). The relative permeability and capillary pressure models were initially developed for partially saturated sediments, but they can also be used to model fluid flow in hydrate systems with minor modifications depending on hydrate saturation [*Dai and Santamarina*, 2013; *Dai and Seol*, 2014]. We use IGSs of 2%, appropriate to porous flow in gas hydrate bearing geologic systems [e.g. *Liu and Flemings*, 2007; *Thatcher et al*., 2013], and 0%, which may be appropriate for purely fracture flow. The anaerobic oxidation of methane in the sulfate reduction zone can consume between 10 and 20% (for high fluid flow rates) and 80% (for lower rates) of dissolved methane approaching the seabed [*Boetius and Wenzhöfer*, 2013]. We represented the effects of this process by including in our starting models a methane-free zone close to the seabed, in which methane approaching the seabed dissolves. This approach likely over-estimates methane consumption at the base of the methane-free zone initially, but perhaps underestimates methane consumption close to the seabed at later times, as methane concentrations build up. Following *Zeebe* [2013], we used a thickness of 20 m for the methane-free zone.

We assumed an initial hydrate saturation of ~5% between the methane-free zone and the hydrate stability limit, which is representative of estimated saturations beneath the modern ocean [e.g., *Milkov*, 2004; *Thatcher et al.*, 2013]. We used a similar seabed temperature function to that of *Zeebe* [2013], but considered only his initial temperature rise of 5 °C at the PETM onset, with an initial deep ocean temperature of 11 °C. Following this initial

175 temperature rise, we maintained the seabed temperature at a constant value until the end of
176 the model runs after 20 kyr (Figure 1). We considered two alternative durations for the initial
177 temperature rise: 6 kyr, as used by *Zeebe* [2013], and 0.6 kyr, to explore the effect of a very
178 short duration end-member. To capture the range of possible behaviors, we also ran models
179 for two different water depths: 1750 m, where the hydrate stability zone (HSZ) is thick (~150
180 m) and hydrate remains stable at the seabed at maximum PETM temperatures; and 1100 m,
181 where the hydrate stability zone is thin (~30 m) and hydrate is stable at the seabed before
182 warming begins but becomes unstable during the initial PETM temperature rise (Figure 2).
183 We imposed a basal heat flow of 56 mW $m^{-2}$ to obtain initial thicknesses of the GHSZ that
184 match those of *Zeebe* [2013].
185
186 At 1750 mwd (m water depth) hydrate dissociation peaks ~1 kyr and 6 kyr after the initial
187 temperature rise, for 0.6 kyr and 6 kyr warming periods respectively, before dropping to zero
188 as the hydrate is exhausted. At 1100 mwd these peaks are 0.2 and 1.2 kyr after the initial
189 warming. For a 0.6 kyr warming period, hydrate dissolution due to increased methane
190 solubility at higher temperatures [*Waite et al.*, 2009], occurs initially throughout almost the
191 entire HSZ and reaches a maximum at the top of the HSZ (Figure 3a, c). Hydrate dissociation
192 occurs at the base of the HSZ, and starts earlier for 1100 mwd because hydrate is present in a
193 much thinner zone (Figure 3a, c). The dissociation rate is over an order of magnitude greater
194 than the rate of hydrate dissolution (Figure 3c). With this very rapid warming and when the
195 HSZ is thin, similar rates of hydrate dissociation can occur on the top and bottom of the HSZ
196 with lower rates occurring in between (Figure 3a). This behavior may also occur in modern
197 hydrate systems affected by ocean warming [*Marin-Moreno et al.*, 2015b]. For a warming
198 period of 6 kyr, hydrate dissolution does not occur and dissociation starts at the base of the
199 HSZ. This relatively slow warming rate allows hydrate re-formation from the ascent of

methane released by hydrate dissociation below (Figure 3b, d). Note that intrinsic permeability and IGS do not influence the rates of hydrate dissociation and dissolution and only influence the rate of hydrate re-formation. Therefore, the results presented in Figure 3 are very similar to those obtained in the other cases modeled.

A striking result from our study is that in all cases, hydrate dissociation and methane generation in the sediment column is poorly related to methane release to the ocean, both in timing and in magnitude (Figure 2). The models with an intrinsic permeability of $10^{-16}$ $m^2$ show zero emissions over the 20 kyr duration of our runs. For the models with an intrinsic permeability of $10^{-13}$ $m^2$, gas escape into the ocean is delayed by 0.3-3 kyr and 2-8 kyr after gas is generated by hydrate dissociation, for the 1100 and 1750 mwd models respectively. This delay results from the slow vertical rise of gas when it is close to the IGS, and increases as the IGS increases (Figure 2). It decreases as intrinsic permeability increases, but changes little for permeabilities greater than $10^{-13}$ $m^2$ [*Thatcher et al.,* 2013]. This result is important because the delay limits the potential for positive feedback between hydrate dissociation and climate change. For an IGS of 2%, methane release into the ocean is spread over a long period of time: 7-8 kyr for 1100 mwd and 3-4 kyr for 1750 mwd. The shorter duration at 1750 mwd, despite the thicker HSZ, occurs because a larger amount of released methane is present as free gas, which increases the relative permeability for gas and hence the rate of methane ascent. If this saturation threshold is removed, the duration of flow is reduced to 300-800 years, and the variation with water depth is more complex. Importantly, at least half of the methane released by dissociation remains in solution or as gas bubbles beneath the seabed at the end of these model runs (Figure 2). Dissolution occurs within the initially methane-free sulfate reduction zone, but also elsewhere because of the solubility increase due to warming. For an IGS of 2%, more methane remains beneath the seabed as gas bubbles

below that threshold, and less than 15% of the dissociated methane escapes to the ocean (Figure 2).

## 3. Discussion and Conclusions

The delays in methane release associated with thermal diffusion to the seabed have been pointed out before [e.g., *Dickens et al.*, 1995; *Zeebe*, 2013]. However, our analysis shows that there are additional mechanisms that both slow and reduce the methane release into the ocean. These mechanisms operate also in the modern ocean [*Stranne et al.*, 2016]. The delays will be less and emissions more complete in shallower water, with higher geothermal gradient and with a thinner methane-free zone, and vice versa. The different responses of the different parts of the system will result in a net long slow rise in emissions followed by a long slow decline. More rapid escape to the ocean might be triggered by catastrophic slumping, but such events would need to occur globally over a millennial timescale to dominate the global flux into the ocean [*Nisbet et al.*, 2009]. If such catastrophic mechanisms are excluded, and our model runs are broadly representative, then the CIE can be explained by hydrate dissociation only if (i) fractures were present or formed during hydrate dissociation to enhance the permeability and (ii) the minimum hydrate inventory is at least double the c. 2000 PgC [e.g., *Dickens et al.*, 1995] required to account for the CIE based on isotopic mass balance considerations. Given a warm Paleocene ocean and therefore a more restricted hydrate stability field than at present, such a large hydrate inventory is difficult to reconcile with model-based estimates of the modern inventory of c. 550-3000 PgC [*Buffett and Archer*, 2004; *Kretschmer et al.*, 2015; *Piñero et al.*, 2013; *Yamamoto et al.,* 2014]. These inventories might be reconciled if the modern inventory is under-estimated by models [*Beaudoin et al.,* 2014] and/or if higher seabed temperatures stimulated significantly greater methanogenesis in the late Paleocene than today [*Gu et al.*, 2011].

We conclude the following:

1. Rapid warming of the deep ocean, such as during the PETM, can lead to rapid hydrate dissociation, but methane release to the ocean is delayed significantly by transport processes through the hydrate stability field.
2. In our models, most of the methane released from hydrate remains in the sediment pores, as dissolved methane or as free gas and only a small fraction reaches the ocean.
3. To explain the global carbon isotopic excursion at the PETM onset, the global hydrate inventory needs to be significantly larger than that required for isotopic mass balance and the permeability of the sediments needs to be enhanced by fractures.
4. Global PETM warming may well have resulted in hydrate dissociation and release of methane to the global ocean but our results raise further challenges around the mechanism of these processes.

**Acknowledgments**

We thank Gerald Dickens and an anonymous reviewer for their thoughtful comments that considerably improved the quality of the manuscript. TAM and PAW were supported by Royal Society Wolfson Research Merit awards. HMM was partly supported by the TALENTS FVG Programme - Activity 1 - Incoming mobility scheme - European Social Fund, Operational Programme 2007-2013, Objective 2 Regional Competitiveness and Employment, Axis 5 Transnational cooperation". DIAM was supported by a Natural Environment Research Council PhD studentship (NERC grant number: NE/J500112/1). The data used in this paper are published in the cited sources and the code used is available via http://esd1.lbl.gov/research/projects/tough/software/.

**References**


Archer, D., and B. Buffett (2005), Time-dependent response of the global ocean clathrate reservoir to climatic and anthropogenic forcing, *Geochem. Geophys. Geosyst.*, *6*, doi: 10.1029/2004GC000854.

Archer, D., and V. Brovkin (2008), The millennial atmospheric lifetime of anthropogenic CO2, *Climatic Change*, *90*(3), 283-297.

Beaudoin, Y. C., W. Waite, R. Boswell and S. R. Dallimore (Eds.) (2014), *Frozen Heat: A UNEP Global Outlook on Methane Gas Hydrates*, vol. 1, 77 pp., United Nations Environmental Programme, GRID-Arendal, Norway.

Berndt, C., et al. (2014), Temporal Constraints on Hydrate-Controlled Methane Seepage off Svalbard, *Science*, *343*(6168), 284-287.

Boetius, A., and F. Wenzhöfer (2013), Seafloor oxygen consumption fuelled by methane from cold seeps, *Nature Geoscience*, *6*(9), 725-734.

Buffett, B., and D. Archer (2004), Global inventory of methane clathrate: sensitivity to changes in the deep ocean, *Earth and Planetary Science Letters*, *227*(3), 185-199.

Cui, Y., L. R. Kump, A. J. Ridgwell, A. J. Charles, C. K. Junium, A. F. Diefendorf, K. H. Freeman, N. M. Urban, and I. C. Harding (2011), Slow release of fossil carbon during the Palaeocene-Eocene Thermal Maximum, *Nature Geoscience*, *4*(7), 481-485.

Dai, S., and J. C. Santamarina (2013), Water retention curve for hydrate-bearing sediments, *Geophysical Research Letters*, *40*(21), 5637-5641.

Dai, S., and Y. Seol (2014), Water permeability in hydrate-bearing sediments: A pore-scale study, *Geophysical Research Letters*, *41*(12), 4176-4184.

Daigle H. & B. Dugan (2010), Origin and evolution of fracture-hosted methane hydrate deposits. *Journal of Geophysical Research-Solid Earth 115*, B11103, 11101-11121, doi: 10.1029/2010jb007492.

Darnell, K. N., and P. B. Flemings (2015), Transient seafloor venting on continental slopes from warming-induced methane hydrate dissociation, *Geophysical Research Letters*, *42*, doi: 10.1002/2015GL067012.

DeConto, R. M., S. Galeotti, M. Pagani, D. Tracy, K. Schaefer, T. Zhang, D. Pollard, and D. J. Beerling (2012), Past extreme warming events linked to massive carbon release from thawing permafrost, *Nature*, *484*(7392), 87-91.

Dickens, G. R. (2011), Down the Rabbit Hole: toward appropriate discussion of methane release from gas hydrate systems during the Paleocene-Eocene thermal maximum and other past hyperthermal events, *Climate of the Past*, *7*(3), 831-846.

Dickens, G. R., J. R. O'Neil, D. K. Rea, and R. M. Owen (1995), Dissociation of oceanic methane hydrate as a cause of the carbon isotope excursion at the end of the Paleocene, *Paleoceanography*, *10*(6), 965-971.

Dunkley Jones, T., D. J. Lunt, D. N. Schmidt, A. Ridgwell, A. Sluijs, P. J. Valdes, and M. Maslin (2013), Climate model and proxy data constraints on ocean warming across the Paleocene-Eocene Thermal Maximum, *Earth-Science Reviews*, *125*, 123-145.

Foster, L. C., D. N. Schmidt, E. Thomas, S. Arndt, and A. Ridgwell (2013), Surviving rapid climate change in the deep sea during the Paleogene hyperthermals, *Proceedings of the National Academy of Sciences*, *110*(23), 9273-9276.

Gu, G. S., G. R. Dickens, G. Bhatnagar, F. S. Colwell, G. J. Hirasaki, and W. G. Chapman (2011), Abundant Early Palaeogene marine gas hydrates despite warm deep-ocean temperatures, *Nature Geoscience*, *4*(12), 848-851.

Katz, M. E., B. S. Cramer, G. S. Mountain, S. Katz, and K. G. Miller (2001), Uncorking the bottle: What triggered the Paleocene/Eocene thermal maximum methane release?, *Paleoceanography*, *16*(6), 549-562.

Kretschmer, K., A. Biastoch, L. Rüpke, and E. Burwicz (2015), Modeling the fate of methane hydrates under global warming, *Global Biogeochemical Cycles*, *29*(5), 610-625.

Littler, K., U. Röhl, T. Westerhold, and J. C. Zachos (2014), A high-resolution benthic stable-isotope record for the South Atlantic: Implications for orbital-scale changes in Late Paleocene, Early Eocene climate and carbon cycling, *Earth and Planetary Science Letters*, *401*, 18-30.

Liu, X., and P. B. Flemings (2007), Dynamic multiphase flow model of hydrate formation in marine sediments, *Journal of Geophysical Research: Solid Earth 112*(B3), doi: 10.1029/2005JB004227.

Marín-Moreno, H., T. A. Minshull, G. K. Westbrook, B. Sinha, and S. Sarkar (2013), The response of methane hydrate beneath the seabed offshore Svalbard to ocean warming during the next three centuries, *Geophysical Research Letters*, *40*, 5159-5163.

Marín-Moreno, H., M. Giustiniani, M., and U. Tinivella (2015a), The Potential Response of the Hydrate Reservoir in the South Shetland Margin, Antarctic Peninsula, to Ocean Warming over the 21st Century, *Polar Research*, 34, 27443, doi: 10.3402/polar.v34.27443.

Marin-Moreno, H., T. A. Minshull, G. K. Westbrook, and B. Sinha (2015b), Estimates of future warming-induced methane emissions from hydrate offshore west Svalbard for a range of climate models, *Geochem. Geophys. Geosyst.*, *16*(5), 1307-1323.

Milkov, A. V. (2004), Global estimates of hydrate-bound gas in marine sediments: how much is really out there?, *Earth-Science Reviews*, *66*(3), 183-197.

Moridis, G., and K. Pruess (1995), *Flow and Transport Simulations Using T2CG1, a Package of Conjugate Gradient Solvers for the TOUGH2 Family of Codes*, Lawrence Berkeley Laboratory Report LBL-36235, Berkeley, CA.

Moridis, G. J., Y. Seol, and T. Kneafsey (2005), Studies of reaction kinetics of methane hydrate dissociation in porous media, paper 1004 in *Proceedings of the 5th International*

*Conference on Gas Hydrates*, Trondheim, Norway, 12–16 June.

Moridis, G. J., M. B. Kowalsky, and K. Pruess (2012), *TOUGH+HYDRATE v1.2 user's manual: A code for the simulation of system behaviour in hydrate-bearing geological media*, Per. LBNL-0149E, Lawrence Berkeley Natl. Lab., Berkeley, California.

Narasimhan, T.N., and P.A. Witherspoon (1976), An Integrated Finite Difference Method for Analyzing Fluid Flow in Porous Media, *Water Resources Research*, 12(1), 57– 64.

Nisbet, E. G., S. M. Jones, J. Maclennan, G. Eagles, J. Moed, N. Warwick, S. Bekki, P. Braesicke, J. A. Pyle, and C. M. R. Fowler (2009), Kick-starting ancient warming, *Nature Geoscience*, *2*(3), 156-159.

Panchuk, K., A. Ridgwell, and L. R. Kump (2008), Sedimentary response to Paleocene-Eocene Thermal Maximum carbon release: A model-data comparison, *Geology*, *36*(4), 315-318.

Phrampus, B. J., and M. J. Hornbach (2012), Recent changes to the Gulf Stream causing widespread gas hydrate destabilization, *Nature*, *490*(7421), 527-530.

Phrampus, B. J., M. J. Hornbach, C. D. Ruppel, and P. E. Hart (2014), Widespread gas hydrate instability on the upper U.S. Beaufort margin, *Journal of Geophysical Research: Solid Earth*, *119*(12), 8594-8609.

Piñero, E., M. Marquardt, C. Hensen, M. Haeckel, and K. Wallmann (2013), Estimation of the global inventory of methane hydrates in marine sediments using transfer functions, *Biogeosciences*, *10*(2), 959-975.

Reagan, M. T., and G. J. Moridis (2007), Oceanic gas hydrate instability and dissociation under climate change scenarios, *Geophysical Research Letters*, *34*(22), doi:10.1029/2007GL031671.

Sexton, P. F., R. D. Norris, P. A. Wilson, H. Palike, T. Westerhold, U. Rohl, C. T. Bolton, and S. Gibbs (2011), Eocene global warming events driven by ventilation of oceanic dissolved organic carbon, *Nature*, *471*(7338), 349-+.

Sluijs, A., H. Brinkhuis, S. Schouten, S. M. Bohaty, C. M. John, J. C. Zachos, G.-J. Reichart, J. S. Sinninghe Damste, E. M. Crouch, and G. R. Dickens (2007), Environmental precursors to rapid light carbon injection at the Palaeocene/Eocene boundary, *Nature*, *450*(7173), 1218-1221.

Stone, H. (1970), Probability model for estimating three-phase relative permeability, *J. Pet. Technol.*, *22*(2), 214-218.

Stranne, C., M. O'Regan, G. R. Dickens, P. Crill, C. Miller, P. Preto, and M. Jakobsson (2016), Dynamic simulations of potential methane release from East Siberian continental slope sediments, *Geochem. Geophys. Geosyst.*, *17*, 872-886, doi:810.1002/2015GC006119.

Svensen, H., S. Planke, A. Malthe-Sorenssen, B. Jamtveit, R. Myklebust, T. Rasmussen Eidem, and S. S. Rey (2004), Release of methane from a volcanic basin as a mechanism for initial Eocene global warming, *Nature*, *429*(6991), 542-545.

Thatcher, K. E., G. K. Westbrook, S. Sarkar, and T. A. Minshull (2013), Methane release from warming-induced hydrate dissociation in the West Svalbard continental margin: Timing, rates, and geological controls, *Journal of Geophysical Research: Solid Earth*, *118*(1), 22-38.

Thomas, D. J., J. C. Zachos, T. J. Bralower, E. Thomas, and S. Bohaty (2002), Warming the fuel for the fire: Evidence for the thermal dissociation of methane hydrate during the Paleocene-Eocene thermal maximum, *Geology*, *30*(12), 1067-1070.

Van Genuchten, M. T. (1980), A closed-form equation for predicting the hydraulic conductivity of unsaturated soils, *Soil Sc. Soc. Am. J.*, *44*(5), 892-898.

Waite, W. F., et al. (2009), Physical properties of hydrate-bearing sediments, *Rev. Geophys.*, *47*.

Westbrook, G. K., K. E. Thatcher, E. J. Rohling, A. M. Piotrowski, H. Palike, A. H. Osborne, E. G. Nisbet, T. A. Minshull, M. Lanoiselle, and R. H. James (2009), Escape of methane gas from the seabed along the West Spitsbergen continental margin, *Geophysical Research Letters*, *36*(15), L15608, doi:15610.11029/12009GL039191.

Wright, J. D., and M. F. Schaller (2013), Evidence for a rapid release of carbon at the Paleocene-Eocene thermal maximum, *Proceedings of the National Academy of Sciences*, *110*(40), 15908-15913.

Xu T., Y. Ontoy, P. Molling, N. Spycher, M. Parini and K. Pruess (2004), Reactive transport modeling of injection well scaling and acidizing at Tiwi field, Philippines. *Geothermics* *33*(4), 477-491.

Xu, W., R. P. Lowell, and E. T. Peltzer (2001), Effect of seafloor temperature and pressure variations on methane flux from a gas hydrate layer: Comparison between current and late Paleocene climate conditions, *Journal of Geophysical Research: Solid Earth*, *106*(B11), 26413-26423.

Yamamoto, A., Y. Yamanaka, A. Oka, and A. Abe-Ouchi (2014), Ocean oxygen depletion due to decomposition of submarine methane hydrate, *Geophysical Research Letters*, *41*(14), 5075-5083, doi:10.1002/2014GL060483.

Zachos, J. C., G. R. Dickens, and R. E. Zeebe (2008), An early Cenozoic perspective on greenhouse warming and carbon-cycle dynamics, *Nature*, *451*(7176), 279-283.

Zachos, J. C., S. M. Bohaty, C. M. John, H. McCarren, D. C. Kelly, and T. Nielsen (2007), The Palaeocene-Eocene carbon isotope excursion: constraints from individual shell planktonic foraminifer records, *365*(1856), 1829-1842.

Zachos, J. C., et al. (2005), Rapid acidification of the ocean during the Paleocene-Eocene thermal maximum, *Science*, *308*(5728), 1611-1615.

Zeebe, R. E. (2013), What caused the long duration of the Paleocene-Eocene Thermal Maximum?, *Paleoceanography*, *28*(3), 440-452.

Zeebe, R. E., J. C. Zachos, and G. R. Dickens (2009), Carbon dioxide forcing alone insufficient to explain Palaeocene-Eocene Thermal Maximum warming, *Nature Geoscience*, *2*(8), 576-580.

Zeebe, R. E., A. Ridgwell, and J. C. Zachos (2016), Anthropogenic carbon release rate unprecedented during the past 66 million years, *Nature Geoscience*, *9*(4), 325-329.

## Figures

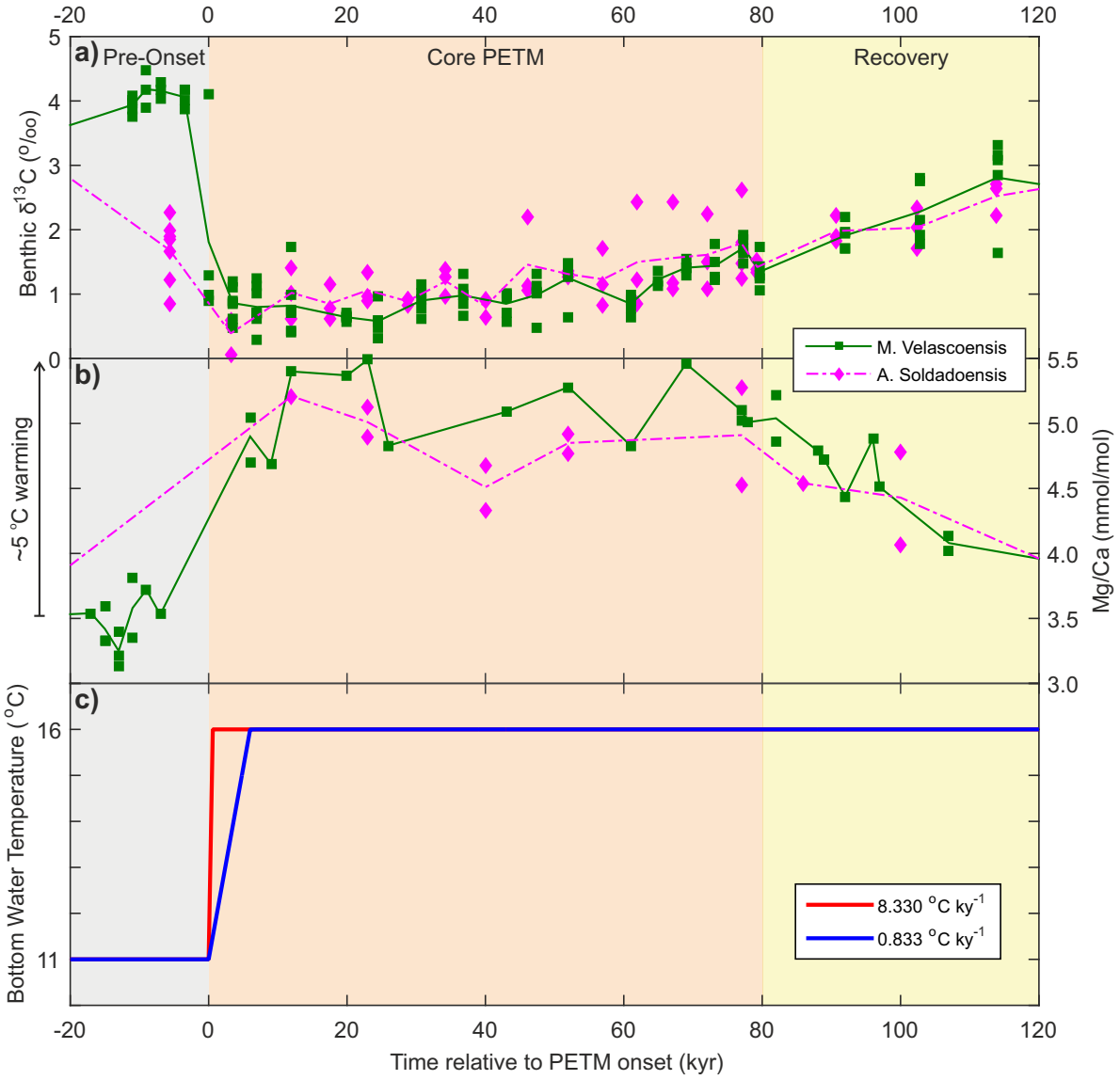


Figure 1. Abrupt warming and carbon cycle perturbation across the PETM revealed in (a) $\delta^{13}C$ [*Zachos et al.*, 2003; with age model of *Penman et al.*, 2014] and (b) Mg/Ca [*Penman et al.*, 2014] data from planktic foraminifera (*Morozovella velascoensis*: green squares and solid line for average; and *Acaranina soldadoensis*: magenta diamonds and dot-dash line for average) from ODP Site 1209 (N. Pacific) revealing a ~3 ‰ carbon isotope excursion and a ~5 °C warming respectively. Panel (c) illustrates the two bottom water temperature functions (a 5 °C increase over either 0.6 kyr (8.330 °C $ky^{-1}$) or 6 kyr (0.8330 °C $ky^{-1}$)) used in this

study. Grey shading indicates the pre-PETM baseline, orange shading the core of the PETM, and yellow shading the post-PETM recovery.

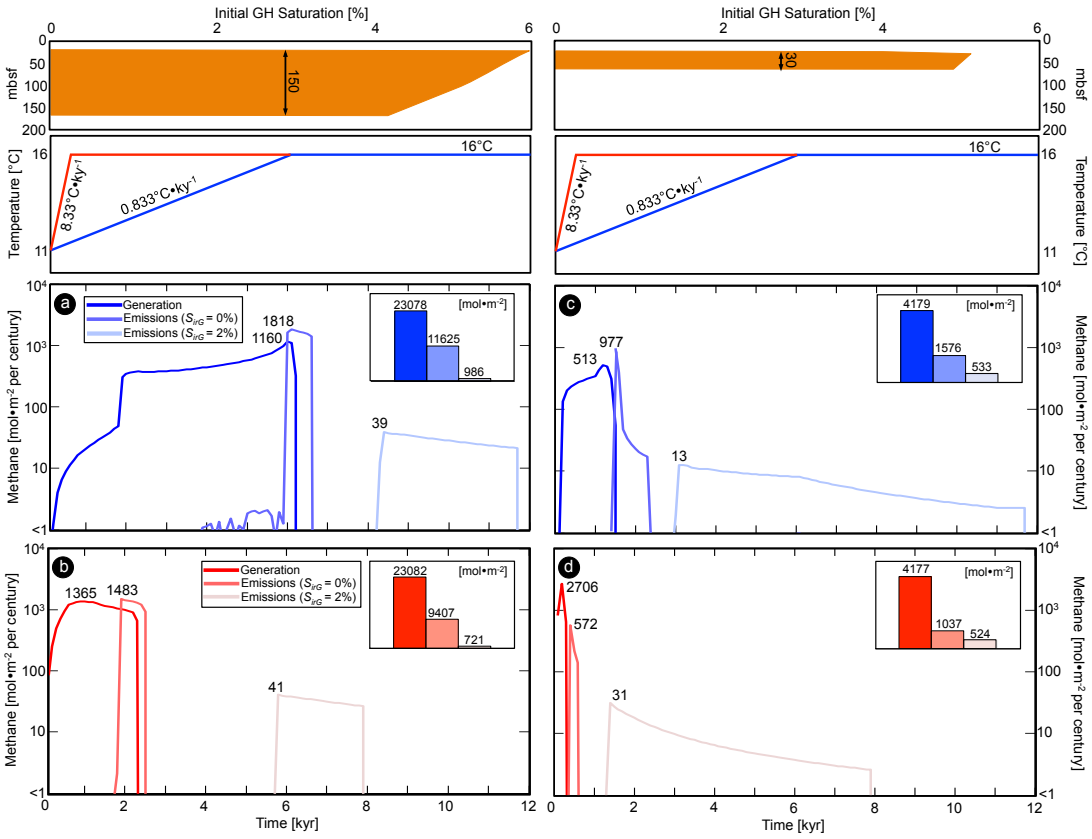


Figure 2. Methane generation from hydrate dissociation (thick lines) and associated seabed methane emissions for an intrinsic permeability of $10^{-13}$ $m^2$, irreducible gas saturations of 0% (medium lines) and 2% (pale lines) and for 0.833 $^oC\ ky^{-1}$ warming (blue) and 8.330 $^oC\ ky^{-1}$ warming (red). Panels (a) and (b) for simulations with a 150 m-thick hydrate layer; panels (c) and (d) for simulations with a 30 m-thick hydrate layer. Note that the vertical scale is logarithmic Histograms show total methane generation and emissions.

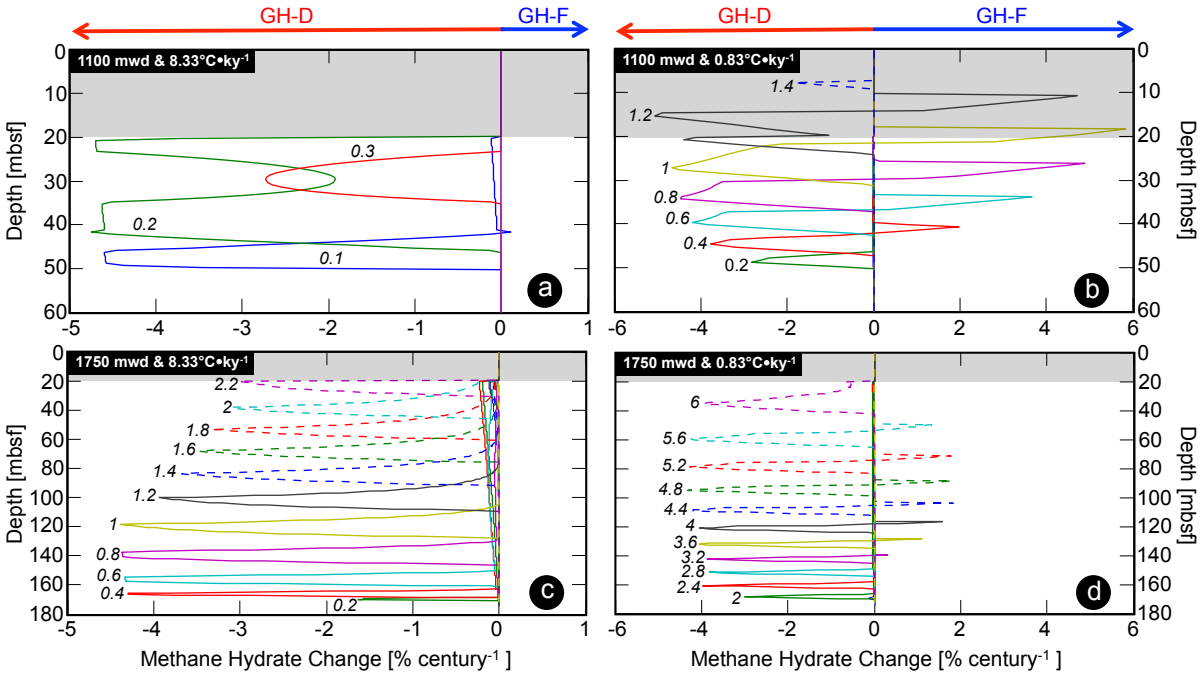


452

453 Figure 3: Rate of hydrate dissociation and/or dissolution (GH-D) and hydrate formation (GH-

454 F) at different times (indicated by the values in kyr next to each line), for models with an

455 intrinsic permeability of $10^{-13}$ $m^2$ and irreducible gas saturation of 2%. (a and b) Results for a

456 30 m hydrate layer for a warming rate of (a) 8.33 C $kyr^{-1}$ and (b) 0.833 C $kyr^{-1}$. (c) and (d)

457 show equivalent plots for a 150 m hydrate layer. In a) and c), the relatively sharp peaks

458 represent dissociation, while the parts of the curves with negative values that slowly increase

459 towards the seabed represent dissolution.

*Geophysical Research Letters*

Supporting Information for

# Mechanistic insights into a hydrate contribution to the Paleocene-Eocene carbon cycle perturbation from coupled thermohydraulic simulations

T. A. Minshull[1*], H. Marín-Moreno[2,3], D. I. Armstrong M[c]Kay[1,4] and P. A. Wilson[1]

[1]National Oceanography Centre Southampton, University of Southampton, Southampton, UK

[2]Istituto Nazionale di Oceanografia e di Geofisica Sperimentale, Trieste, Italy

[3]National Oceanography Centre, Southampton, UK.

[4]Geography and Environment, University of Southampton, Southampton, SO17 1BJ, UK

[*]Corresponding author email: tmin@noc.soton.ac.uk

## Contents of this file

Text S1

Table S1

## Introduction

Text S1 gives some details about the TOUGH+Hydrate code, and the assumptions and parameters used in the model.

Table S1 gives further model parameters that are not given in the text, and the sources of these parameters.

**Text S1. Modeling approach**

We employ TOUGH+ Hydrate (T+H), a thermohydraulic numerical code for the simulation of the behavior of gas hydrate bearing sediments under non-isothermal conditions. Here we describe the most important physical processes modeled and assumptions considered; detailed information about the mathematical formulation is available from the online T+H manual (*http://esd.lbl.gov/files/research/projects/tough/documentation/ TplusH_Manual_v1. pdf*). Following previous studies [e.g. *Reagan and Moridis*, 2007; *Thatcher et al*., 2013], methane and water relative permeabilities were computed according to a modified version of *Stone*'s [1970] first three-phase relative permeability method and the capillary pressure was calculated using *van Genuchten*'s [1980] law (Table S1). Both models were adjusted using the Evolving Porous Medium (EPM) model #2 [*Moridis et al*., 2012]. The relative permeability model was adjusted for changes in the saturation of solid phases (ice or hydrate) occupying the pore space. The capillary pressure model was adjusted for both changes in porosity, resulting from changes in pressure and in saturation of solid phases in the pores, and changes in intrinsic and relative permeabilities, resulting from changes in porosity (Table S1). In our runs, changes in porosity due to changes in pressure (Table S1) are almost negligible.

For each model we performed an initialization run to establish steady-state initial pressure, temperature, and gas hydrate distribution conditions (in this initialization run molecular diffusion was not considered). To obtain an initial temperature profile with a

geothermal gradient of 37.3°C $km^{-1}$, similar to the initial geothermal gradient used by *Zeebe* [2013] of 37-40 °C $km^{-1}$, we (i) imposed the initial seabed temperature on the top cell of 11 °C and a heat flow source on the bottom cell of $5.6x10^{-2}$ W $m^{-2}$, (ii) assumed a sediment thermal conductivity in fully water saturated conditions of 1.5 W $m^{-1}K^{-1}$ and a porosity of 40% [*Zeebe*, 2013], and (iii) ran the model long enough to achieve convergence (steady-state conditions). We imposed the heat flow instead of geothermal gradient because the latter changes with the phase (water, gas, hydrate and ice) occupying the pore space

To model warming-induced hydrate dissociation, we initialized the models using the steady-state pressure, temperature and gas hydrate distribution profiles obtained during the initialization runs, and step-changed the temperature of the top cell (representing the seabed) every 100 yrs while keeping a constant source of heat flow at the bottom of the model equal to that used during the initialization process. The heat supply by seabed temperature changes does not have sufficient time to diffuse down and reach the deeper part of the model (at 1 km below seabed). Thus, the bottom temperature remains constant even without considering the heat flow source at the base. However, when hydrate disappears completely and giving sufficient time, this source of heat allows recovering the initial steady-state geothermal gradient of 37.3 °C $km^{-1}$ in the entire column. We also considered a fully water saturated thermal conductivity and an initial porosity equal to those used during the initialization runs (Table S1).

It is unlikely that very low permeability can be maintained in marine sediments when gas is being produced rapidly from hydrate dissociation [e.g. *Stranne et al*., 2016], because, for an intrinsic permeability of about $10^{-16}$ $m^2$, the pore pressure exceeds the lithostatic load only a few years after the dissociation of hydrate commences [*Thatcher et al*., 2013]. Consequently, fractures are likely to form and fluid flow to become dominated by the greater permeability of the fractures, rather than the original intergranular permeability of the sediments in which they occur. The approach of *Marín-Moreno et al.* [2015a] and *Stranne et al*. [2016] does not consider pre-existing fractures in the system before hydrate dissociation. Therefore, here we prefer the enhanced permeability approach justified in detail by *Thatcher et al.* [2013] that implicitly embodies the assumption that shallow fractures are present. A value of $10^{-13}$ $m^2$ was required to explain observed warming-induced methane emissions in the continental margin offshore west of Svalbard, where fractures have been seismically interpreted [*Thatcher et al.,* 2013]. For intrinsic permeabilities greater than $10^{-13}$ $m^2$ our general statements regarding the onset of methane emissions are still valid because the rate of free methane gas transport from dissociated hydrate to the seabed is then limited by the rate at which the latent heat required to dissociate hydrate can be supplied [*Marín-Moreno et al.*, 2013; *Thatcher et al.,* 2013]

The 1D models have a total thickness of 1.005 km with a constant cell size of 0.5 m except for the top cell (where the top boundary condition is imposed) that has a thickness of 0.005 m. Convergence is achieved when the norm of the ratio of the residuals from the Newton-Raphson iteration with respect to the accumulation term, which includes mass

and heat components, is below a convergence tolerance assume here to be $10^{-5}$. When the accumulation term is below 1, an absolute convergence criterion is applied and convergence is achieved when the norm of the residuals is below $10^{-5}$.

**References**


Marín-Moreno, H., T. A. Minshull, G. K. Westbrook, B. Sinha, and S. Sarkar (2013), The response of methane hydrate beneath the seabed offshore Svalbard to ocean warming during the next three centuries, *Geophysical Research Letters*, 2013GL057912, doi: 10.1002/grl.50985.

Marín-Moreno, H., Giustiniani, M., and Tinivella, U. (2015a), The Potential Response of the Hydrate Reservoir in the South Shetland Margin, Antarctic Peninsula, to Ocean Warming over the 21st Century, *Polar Research*, 34, 27443, doi: 10.3402/polar.v34.27443.

Marín-Moreno H., Minshull T. A., Westbrook G. K. and Sinha B. (2015b), Estimates of future warming-induced methane emissions from hydrate offshore West Svalbard for a range of climate models, *Geochemistry, Geophysics, Geosystems*, n/a-n/a, doi: 10.1002/2015gc005737.

Moridis, G. J., Y. Seol, and T. Kneafsey (2005), Studies of reaction kinetics of methane hydrate dissociation in porous media, paper 1004 in *Proceedings of the 5th International Conference on Gas Hydrates*, Trondheim, Norway, 12–16 June.

Moridis, G. J., M. B. Kowalsky, and K. Pruess (2012), TOUGH+HYDRATE v1.2 user's manual: A code for the simulation of system behavior in hydrate-bearing geological media, Per. LBNL-0149E, Lawrence Berkeley Natl. Lab., Berkeley, Calif.

Reagan, M. T., and G. J. Moridis (2007), Oceanic gas hydrate instability and dissociation under climate change scenarios, *Geophysical Research Letters*, *34*(22), doi:10.1029/2007GL031671.

Stone, H. (1970), Probability model for estimating three-phase relative permeability, *J. Pet. Technol.*, *22*(2), 214-218.

Stranne, C., O'Regan, M., Dickens, G.R., Crill, P., Miller, C., Preto, P., Jakobsson, M. (2016), Dynamic simulations of potential methane release from East Siberian continental slope sediments. *Geochemistry, Geophysics, Geosystems* 17, 872-886, doi: 10.1002/2015GC006119

Thatcher, K. E., G. K. Westbrook, S. Sarkar, and T. A. Minshull (2013), Methane release from warming-induced hydrate dissociation in the West Svalbard continental margin: Timing, rates, and geological controls, *Journal of Geophysical Research: Solid Earth*, *118*(1), 22-38, doi: 10.1029/2012jb009605.

van Genuchten, M. T. (1980), A closed-form equation for predicting the hydraulic conductivity of unsaturated soils, *Soil Sc. Soc. Am. J.*, *44*(5), 892-898, doi: 10.2136/sssaj1980.03615995004400050002x.

Xu T., Y. Ontoy, P. Molling, N. Spycher, M. Parini and K. Pruess (2004), Reactive transport modeling of injection well scaling and acidizing at Tiwi field, Philippines. *Geothermics 33*(4), 477-491, doi: 10.1016/j.geothermics.2003.09.012.

Zeebe, R.E. (2013), What caused the long duration of the Paleocene-Eocene Thermal Maximum?. *Paleoceanography 28*, 440-452, doi: 10.1002/palo.20039.

**Table S1.** Physical properties of the gas hydrate system.

| Parameter | Value | Reference |
|---|---|---|
| Initial salinity [wt%] | 3.5 | [*Thatcher et al.*, 2013] |
| Initial hydrate saturation [vol %] | 5 | [*Thatcher et al.*, 2013] |
| Initial MFZ thickness [m] | 20 | [*Zeebe*, 2013] |
| Gas composition | 100% $CH_4$ | [*Marín-Moreno et al.*, 2013] |
| Heat flow[1] [W $m^{-2}$] | $5.6 \times 10^{-2}$ | [*Zeebe*, 2013] |
| Sediments thermal conductivity in fully water saturated conditions. $k_{Tw}$ [W $m^{-1}K^{-1}$] | 1.5 | [*Zeebe*, 2013] |
| Sediments thermal conductivity in dry conditions $k_{Td}$ [W $m^{-1}K^{-1}$] | 0.55 | [*Marín-Moreno et al.*, 2015] |
| Bulk thermal conductivity of the sediments [W $m^{-1}K^{-1}$] | $k_t = \left(\sqrt{S_h} + \sqrt{S_A}\right) \cdot \left(k_{Tw} - k_{Td}\right) + k_{Td}$ | [*Moridis et al.*, 2005] |
| Solid grain density [kg $m^{-3}$] | 2600 | [*Zeebe*, 2013] |
| Solid grain specific heat [J $kg^{-1}K^{-1}$] | 1000 | [*Zeebe*, 2013] |
| Pore compressibility $\alpha_p$ [$Pa^{-1}$] | $3 \times 10^{-8}$ | [*Marín-Moreno et al.*, 2015] |
| Thermal expansivity $\alpha_T$ [$K^{-1}$] | 0 | |
| Initial porosity $\phi_0$ [%] | 40 | [*Zeebe*, 2013] |
| Porosity function [%] | $\phi = \phi_0 \exp(\alpha_p P + \alpha_T T)$ | [*Moridis et al.,* 2012] |
| Initial intrinsic permeability $k_{i0}$ [$m^2$] | $10^{-13}$, $10^{-16}$ | This study |
| Intrinsic permeability function [$m^2$] | $k_i = k_{i0}\left(\frac{\phi - \phi_c}{\phi_0 - \phi_c}\right)^{n_k}$<br>$\phi_c = 0.05$ ; $n_k = 3$ | [*Xu et al*., 2004] |
| Relative permeability model:<br>Modified version of Stone's first three phase relative permeability method | $k_{rA} = \max\left\{0, \min\left\{\left[\frac{S_A - S_{irA}}{1 - S_{irA}}\right]^n, 1\right\}\right\}$,<br>$k_{rG} = \max\left\{0, \min\left\{\left[\frac{S_G - S_{irG}}{1 - S_{irA}}\right]^{n_G}, 1\right\}\right\}$,<br>$S_{irA} = 0.12$, $S_{irG} = [0.02, 0]$, $n = n_G = 4$ | [*Stone*, 1970] |
| Capillary pressure model | $P_{cap} = -P_0\left[\left(S^*\right)^{-1/\lambda} - 1\right]^{1-\lambda}$,<br>$-P_{\max} \le P_{cap} \le 0$,<br>$S^* = \frac{\left(S_A - S_{irA}\right)}{S_{mxA} - S_{irA}}$,<br>$\lambda = 0.254$, $S_{irA} = 0.11$, $P_0 = 12500$ Pa,<br>$P_{\max} = 10^6$ MPa, $S_{mxA} = 1$ | [*van Genuchten*, 1980] |
| Initial diffusivity [$m^2$ $s^{-1}$] | | [*Marín-Moreno et al*., 2013] |
| $CH_4$: aqueous phase, gas phase | $2 \times 10^{-9}$, $2 \times 10^{-5}$ | |
| $H_2O$: aqueous phase, gas phase | $1 \times 10^{-9}$, $3 \times 10^{-5}$ | |
| NaCl: aqueous phase, gas phase | $1.5 \times 10^{-9}$, 0 | |

[1] Heat flow estimated based on *Zeebe*'s [2013] geothermal gradient and water saturated thermal conductivity.

GHSZ, gas hydrate stability zone; MFZ, methane-free zone; mwd, meters water depth; mbsf, meters below seafloor; $\phi_c$ is critical porosity; $n_k$ is a fitting parameter; $k_{rA}$ and $k_{rG}$ are relative permeabilities for aqueous and gas phases, respectively; $S_A$, $S_G$, and $S_H$ are saturations for aqueous, gas and hydrate phases; $S_{irA}$ and $S_{irG}$ are irreducible aqueous and gas saturations; $S_{mxA}$ is the maximum water saturation; $P$ is the pore pressure; $P_{cap}$ is the capillary pressure; $P_{max}$ is the maximum value of capillary pressure; $P_0$ is the capillary entry pressure; $T$ is the temperature; $n$, $n_G$ and $\lambda$ are fitting parameters.